Universal scaling of the electronic and the elastic energies of small polarons revealed by high-throughput first-principles calculations

Fei Zhou, Babak Sadigh, and Daniel Åberg
Physical and Life Sciences Directorate, Lawrence Livermore National Laboratory, Livermore, California 94550, USA
(Dated: May 23, 2022)

Formation of self-trapped holes (STH) in a comprehensive list of scintillator materials, including halides and chalcogenides, are studied using an accurate and computationally efficient first-principles method, the polaron self-interaction correction (pSIC). The key characteristics of small hole polarons, including their geometries, energies and degree of localization, are found vastly different from halides to oxides to systems with open-shell cations. Nevertheless, we find a universal linear relation between the energy gap separating the bound hole level from the valence band maximum and the elastic energy associated with the lattice displacement field that accompanies the polaron.

PACS numbers: 71.38.Ht,71.15.Mb

Polarons are quasi-particles in semiconductors, consisting of charge carriers (electron/hole) and the surrounding lattice deformation due to electron-phonon coupling [1]. Accurate description of polaron formation and transport is crucial to understanding important quantum mechanical processes occurring in (opto)electrochemical devices such as scintillation detectors, batteries, photovoltaics and light emitting devices. Since the seminal works of Fröhlich [2], great progress has been made in our theoretical understanding of the so-called "large polarons", the extent of which is much larger than the lattice constant [3]. In contrast, "small" or self-trapped polarons with localized charge [4] are more difficult to model, as complex interactions between the localized charge and the immediate surrounding ions dictate the nature of the charge localization and ionic displacement.

First-principles methods prove to be an invaluable tool to predict the properties of small polarons (or just polarons in this work). Since standard density functional (DFT) theory fails to stabilize polaronic states [5, 6], mainly due to the large self-interaction error of the localized state, several alternatives have been suggested. These are either based on introducing a localized potential in the spirit of LDA+U [7–9] or in the case of hybrid functionals by incorporating a certain fraction of possibly screened exchange interaction [5, 6, 10, 11]. Although the dependence on external parameters in both approaches can to some extent be removed by invoking Koopman's theorem, both approaches currently suffer from severe drawbacks. The former are restricted to polarons localized on atomic sites and thus not applicable to V_K-centers (a hole localized on a *dimerized* nearest-neighbor halide-ion pair, see also Fig. 2a) in alkali halides [12], and, as we shall see, other halides and a wide range of oxides. Hybrid functionals do not suffer from this shortcoming, but are computationally expensive, although recent advances have brought about substantial speed-up [13]. Nevertheless, hybrid functional studies of small hole polaron formation were performed in e.g. eight wide-band-gap oxides [14], in $SrTiO_3$ [15, 16], and in TiO_2 [17], and found stable polarons centered on one oxygen atom (*monomer*, see also Fig. 2b). We have recently devised a parameter-free energy functional called the polaron self-interaction correction (pSIC), capable of predicting accurate polaronic structures and binding energies with a computational cost on par with standard DFT [6]. The method was recently used to map out the complete hole polaron migration paths in SrI_2 [18]. Since the major roadblock for atomistic modeling of polarons has been eliminated, we are ready fo larger scale exploration of polaron formation in an efficient and automated manner.

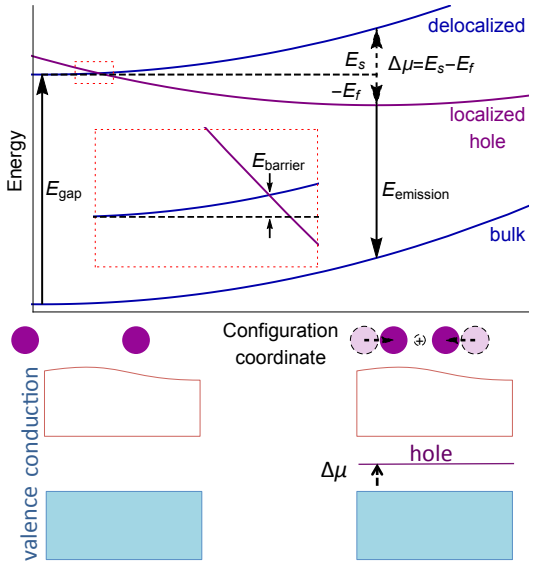

FIG. 1. Top: schematic energy profile for small hole polaron formation, stabilized by $\Delta\mu$, the position of the hole state relative to VBM. Inset shows the static barrier towards charge localization. Bottom: Electronic band structure in ideal and polaronic configuration.

In the following we will present a systematic and comprehensive study of the formation of self-trapped holes (STH) in scintillator materials by high-throughput first-principles calculations. The list of scintillator materi-

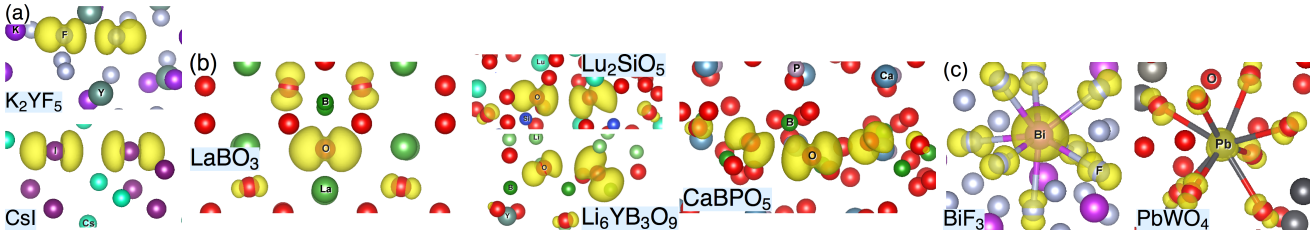

FIG. 2. Hole charge distribution of representative polarons in (a) halides, (b) oxides, and (c) systems with open-shell cations, with isosurface (yellow) of hole charge density at 0.01 e/Å^3.

als was taken from the LBNL scintillator database [19], including 10 fluorides, 13 chlorides, 6 bromides, 7 iodides, 45 oxides, 1 sulfide, as well as 15 mixed-anion compounds, e.g. LaOF (more details in Supplemental Material). With the large amount of computed data, we aim to gain insight beyond the scope of one or a few select materials in order to address the following general questions: (1) Do small hole polarons exist in this class of materials? (2) If so, what are the polaron stability, degree of charge localization and the associated phonon mode? (3) What are the systematic trends and correlation, if any?

The development of the pSIC approach [6] was spurred by the realization that the self-interaction of the localized charge, manifested by the non-zero curvature of the total energy as a function of fractionally charge, is responsible for DFT's failure to stabilize polarons in wide gap insulators. The details can be found in Ref. 6, but we here repeat some of its salient features. The pSIC total energy functional in the Born-Oppenheimer approximation for a system with an added hole is given by

$$E^h_{\rm BO}[\boldsymbol{R}] = E^0_{\rm DFT}[\boldsymbol{R}] - \mu^h_{\rm DFT}[\boldsymbol{R}], \qquad (1)$$

where $E^0_{\rm DFT}[\boldsymbol{R}]$ is the total energy of the ionic configuration $\boldsymbol{R}$ in the neutral charge state, and $\mu^h_{\rm DFT}$ is the hole chemical potential, i.e. the left-derivative of $E^0_{\rm DFT}$ with respect to electron number. We have shown extensively in the past that the pSIC functional can accurately account for the strong coupling of charge excitations to ionic displacements in insulators, leading to formation of bound electron/hole states inside the band gap [6, 18]. Fig. 1 shows schematically the formation of a bound hole state separated from the VBM by $\Delta\mu = \mu^h_{\rm DFT}[\boldsymbol{R}_{\rm pol}] - \mu^h_{\rm DFT}[\boldsymbol{R_0}]$, with $\boldsymbol{R}_0$ and $\boldsymbol{R}_{\rm pol}$ denoting the ideal and the polaronic configurations.

Hole polaron formation or binding energies are

$$E_{\rm B}[\boldsymbol{R}_{\rm pol}] = E^h_{\rm BO}[\boldsymbol{R}_{\rm pol}] - E^h_{\rm BO}[\boldsymbol{R}_0] = E_{\rm s} - \Delta\mu. \qquad (2)$$

The decomposition of $E_{\rm B}$ in Eq. (2) into an elastic contribution $E_{\rm s}$, i.e. the energy cost for the neutral system to deform, and an electronic contribution $\Delta\mu$, which signifies the interaction of the polaron with the lattice, is a good starting point for deriving the non-adiabatic potential-energy barrier for polaron formation within a classical Marcus theory [20]. Hence, let Ψ^h_0 and $\Psi^h_{\rm pol}$ be the free- and bound-hole wavefunctions respectively. In the limit of linear electron-phonon coupling, the bound-hole energy landscape can be written as

$$E^h_{\rm bound}[\boldsymbol{R}] = E^0_{\rm DFT}[\boldsymbol{R}] - \mu^h_{\rm DFT}[\boldsymbol{R}_{\rm pol}] - \left\langle \Psi^h_{\rm pol} \left| \frac{\partial H(\boldsymbol{R}_{\rm pol})}{\partial \boldsymbol{R}} \right| \Psi^h_{\rm pol} \right\rangle \cdot (\boldsymbol{R} - \boldsymbol{R}_{\rm pol}), \qquad (3)$$

while the free-hole energy landscape $E^h_{\rm free}[\boldsymbol{R}]$ can be formulated in the same way, only replacing $\boldsymbol{R}_{\rm pol}$ above with $\boldsymbol{R}_0$, and $\Psi^h_{\rm pol}$ with Ψ^h_0. In practice, we determine the electron-phonon matrix element in Eq. (3) by computing $\frac{\partial \mu^h_{\rm DFT}}{\partial \boldsymbol{R}}$ at $\boldsymbol{R}_{\rm pol}(\boldsymbol{R}_0)$ for the bound(free) hole.

Previous studies of STH in scintillator materials were mainly carried out in relatively simple crystal structures (e.g. rock salt) [6]. Combined with the knowledge of hole polarons localized on halide dimers, such simple structures point unambiguously towards one or few types of polarons on nearest-neighbor anion pairs. Recently we performed a systematic examination of all possible halide dimer configurations within a certain pair distance in SrI_2 [18]. In the present high-throughput study, simply locating nearest-neighbor anion pairs is obviously not enough. First, in many cases the nature of STH is not well established, e.g. mixed halides and oxides. Second, we would like to avoid unnecessary presumption or bias in our search. In the present study, we adopt a different strategy for the search of polaron configurations. First a brief *ab initio* molecular dynamics simulation of the neutral supercell is performed for 1-2 ps in steps of 5 fs, followed by pSIC structural relaxation starting from 6–10 well-separated snapshots of the trajectory. Additionally, pSIC relaxation were performed using up to 10 initial structures generated by randomly and independently displacing by 0.12-0.15 Å every atoms in the ideal supercell. This approach is a compromise between computational efficiency and breadth of the search. All internal degrees of freedom were relaxed until the atomic forces are within 0.02 eV/Å while the cell shape are lattice parameters are fixed at the experimental values. DFT calculations were performed using the Perdew-Becke-Ernzerhof (PBE) [21] parametrization of the Generalized Gradient Approximation (GGA), projector augmented-wave (PAW) potentials [22], and no symmetry constraints as implemented

in the VASP code [23]. For pSIC calculations of polaronic configurations, one hole is embedded in supercells containing about 70-140 atoms in order to achieve sufficient cell size convergence for the present purpose. For each material, we report the most stable polaron configuration found.

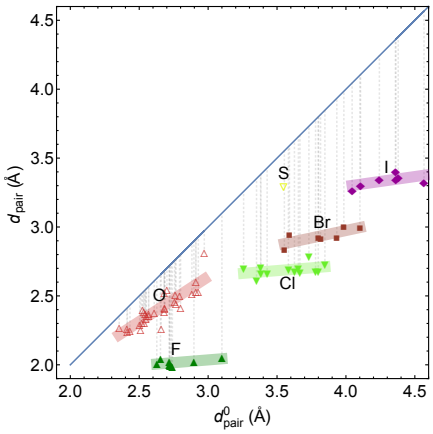

FIG. 3. Dimer pair distance before ($d^0_{\rm dimer}$) and after relaxation ($d_{\rm dimer}$), with gray dashed lines and color bars representing distance contraction and linear regressions, respectively.

We find stable small polarons in most of the considered systems; only in 9 out of 97 considered materials did our search fail to identify any stable hole configuration. Charge distributions of a few representative systems are shown in Fig. 2. To quantify charge localization, we consider the fractional occupancy n_i on atom i of the hole state. Depending on the number of atoms with significant hole occupancy (defined here as $n_i > 0.1$), the obtained polarons are called monomers, dimers or trimers. Similar to V_k centers in alkali halides, dimers involving two neighboring anions are prevalent in other halides (Fig. 2a). A wide range of configurations occur in oxides, with roughly the same number of monomers as dimers, as well as one case of trimer formation in $CaBPO_5$ (Fig. 2b). Stable dimers were found in 11 out of 15 mixed-anion compounds, and the hole oxidizes the less electronegative anion, e.g. Br-Br in BaBrCl, and S-S in LaSCl. Finally, monomers center on open-shell cations, including Bi^{3+} in BiF_3 and Pb^{2+} in $PbWO_4$, increasing their valence (Fig. 2c).

Figure 3 shows the pair distance of the stable dimer configurations. The distance contraction due to polaron structural deformation (gray dashed lines in Fig. 3) is very different between halides an oxides. In each type of halides the distance contracts to approximately the same value: 2.0 Å in fluorides, 2.7 Å in chlorides, 2.9 Å in bromides and 3.3 Å in iodides. The range of the contraction is approximately the same among halide types: 0.5-1.1 Å. In contrast, the contraction among oxides is small and uniform at 0.2-0.3 ÅṪhe only S-S dimer in our study contracts by less than 0.2 Å, similar to oxides.

We now discuss the relation between the kinetics of self-trapping and the polaron binding energy, a typical thermodynamic property. The non-adiabatic transition state surface occurs at $\boldsymbol{R}_{\rm TS}$, the crossing of the bound-hole and the free-hole landscapes. In this work, we only consider the simplest reaction coordinate for self-trapping, i.e. the straight path $\boldsymbol{R}(u) = (1-u)\boldsymbol{R}_0 + u\boldsymbol{R}_{\rm pol}$. The transition state $u_{\rm TS}$ satisfies

$$k_0 u_{\rm TS} + k_{\rm pol}(1 - u_{\rm TS}) = \Delta\mu, \tag{4}$$

where $k_0 = \frac{\partial \mu^h_{\rm DFT}(\boldsymbol{R}_0)}{\partial \boldsymbol{R}} \cdot (\boldsymbol{R}_{\rm pol} - \boldsymbol{R}_0)$, and $k_{\rm pol}$ is defined similarly. Note that the determination of $u_{\rm TS}$ does not involve the elastic energy $E_{\rm s}$. For this purpose, we first consider the Born-Oppenheimer energy landscape of a hole:

$$E^h_{\rm BO}(u) = E_s(u) - \mu^h(u), \tag{5}$$

with $E_s(0) = \mu^h(0) = 0$, $E_s(1) = E^0_{\rm DFT}[\boldsymbol{R}(1)] - E^0_{\rm DFT}[\boldsymbol{R}(0)]$, $\mu^h(1) = \Delta\mu$, $\frac{d\mu^h(1)}{du} = k_{\rm pol}$, and $\frac{d\mu^h(0)}{du} = k_0$. Let us assume a harmonic model for the elastic energy: $E_s(u) = \frac{1}{2}\omega_s^2 u^2$. That the polaron is at equilibrium at $u = 1$ implies that $\omega_s^2 = k_{\rm pol}$. Furthermore, the delocalized nature of the free hole suggests that $k_0 << k_{\rm pol}$ and thus can be neglected (see Supplemental Materials). As a result, Eq. (4) is reduced to $u_{\rm TS} = 1 - \Delta\mu/k_{pol}$. We thus obtain the following two expressions for the *non-adiabatic* kinetic barrier to self-trapping and binding energy:

$$E_{\rm barrier} = \frac{k_{\rm pol}}{2}\left[1 - \frac{\Delta\mu}{k_{\rm pol}}\right]^2, \tag{6}$$

$$E_{\rm B} = \Delta\mu - \frac{k_{\rm pol}}{2}, \tag{7}$$

related by

$$E_{\rm barrier} = \frac{k_{\rm pol}}{2}\left[\frac{E_{\rm B}}{k_{\rm pol}} - \frac{1}{2}\right]^2. \tag{8}$$

The above quadratic relation between $E_{\rm barrier}$ and $E_{\rm B}$ is typical of the classical Marcus theory [20].

We now arrive at the main finding of this paper. It is the discovery of a nearly linear correlation between the electronic $\Delta\mu$ and elastic $E_s(1)$ contributions to the polaron binding energy:

$$\Delta\mu \approx 1.5 E_s(1), \tag{9}$$

as shown in Fig. 4. Since there is no apparent reason for the linear correlation, it is remarkable that materials across different structures and chemistry, including all halides, oxides, mixed-anion, and even across different polaron formation mechanism (open-shell systems with holes localized primarily on cations rather than anions), all obey this simple rule. If we now approximate the elastic energy with the harmonic model, where

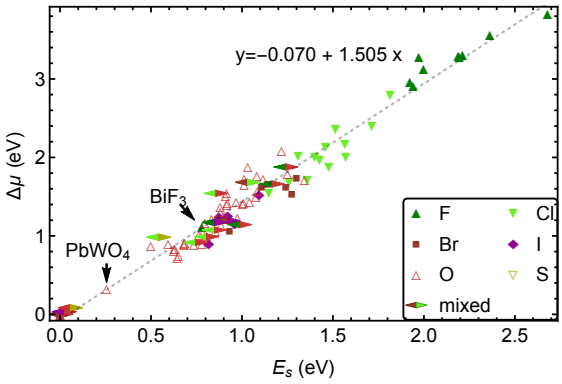

FIG. 4. Comparison of the elastic (ΔE_s) and charge ($-\Delta\mu$) contributions to the binding energy of small hole polarons.

$E_s(1) = \omega_s^2/2 = k_{\rm pol}/2$ as described above, we find a direct proportionality

$$E_{\rm barrier} = \frac{1}{8} E_{\rm B}. \tag{10}$$

In summary, we have carried out high-throughput pSIC calculations to search systematically for hole charge localization and small polaron formation in scintillator materials. In halides, the most common polaron is the symmetric dimer consisting of the X_2^- molecule, with decreasing stability from fluorides to iodide. In oxides the polaron may take the form of monomers, dimers and configurations in between, with more dispersedly distributed hole charge. An universal linear correlation was revealed between the position of the hole states relative to valence band maximum and polaron binding energy.

This work was performed under the auspices of the U.S. Department of Energy by Lawrence Livermore National Laboratory under Contract No. DE- AC52-07NA27344 with the support from the National Nuclear Security Administration Office of Nonproliferation Research and Development (NA-22).

[1] A. S. Alexandrov and J. T. Devreese, *Advances in Polaron Physics*, Springer Series in Solid-State Sciences (Springer, Berlin Heidelberg, 2009).
[2] H. Fröhlich, Adv. Phys. **3**, 325 (1954).
[3] J. T. Devreese and A. S. Alexandrov, Rep. Prog. Phys. **72**, 066501 (2009).
[4] A. M. Stoneham, J. Gavartin, A. L. Shluger, A. V. Kimmel, D. M. Ramo, H. M. Rønnow, G. Aeppli, and C. Renner, J. Phys.: Condens. Matter **19**, 255208 (2007).
[5] J. L. Gavartin, P. V. Sushko, and A. L. Shluger, Phys. Rev. B **67**, 035108 (2003).
[6] B. Sadigh, P. Erhart, and D. Åberg, Phys. Rev. B **92**, 075202 (2015); B. Sadigh, P. Erhart, and D. Aberg, *ibid.* **92**, 199905(E) (2015).
[7] V. I. Anisimov, J. Zaanen, and O. K. Andersen, Phys. Rev. B **44**, 943 (1991).
[8] S. Lany and A. Zunger, Phys. Rev. B **80**, 085202 (2009).
[9] P. Erhart, A. Klein, D. Åberg, and B. Sadigh, Phys. Rev. B **90**, 035204 (2014).
[10] P. Deák, B. Aradi, and T. Frauenheim, Phys. Rev. B **86**, 195206 (2012).
[11] K. Biswas and M.-H. Du, Phys. Rev. B **86**, 014102 (2012).
[12] W. Känzig, Phys. Rev. **99**, 1890 (1955).
[13] M. Guidon, F. Schiffmann, J. Hutter, and J. VandeVondele, J. Chem. Phys. **128**, 214104 (2008).
[14] J. B. Varley, A. Janotti, C. Franchini, and C. G. Van de Walle, Phys. Rev. B **85**, 081109 (2012).
[15] H. Chen and N. Umezawa, Phys. Rev. B **90**, 035202 (2014).
[16] A. Janotti, J. B. Varley, M. Choi, and C. G. van de Walle, Phys. Rev. B **90**, 085202 (2014).
[17] S. Chen and L.-W. Wang, Phys. Rev. B **89**, 014109 (2014).
[18] F. Zhou, B. Sadigh, P. Erhart, and D. Åberg, npj Computational Materials **2**, 16022 (2016).
[19] S. Derenzo, M. Boswell, M. Weber, and K. Brennan, http://scintillator.lbl.gov/ .
[20] R. Marcus, Rev. Mod. Phys. **65**, 599 (1993).
[21] J. P. Perdew, K. Burke, and M. Ernzerhof, Phys. Rev. Lett. **77**, 3865 (1996).
[22] P. E. Blochl, Phys. Rev. B **50**, 17953 (1994).
[23] G. Kresse and D. Joubert, Phys. Rev. B **59**, 1758 (1999).
[24] A. Fonari and C. Sutton, "Effective mass calculator," (2012).